



**HAL**  
open science

# Long-range Energy Transfer Between Dye-loaded Nanoparticles: Observation and Amplified Detection of Nucleic Acids

Deep Sekhar Biswas, Paraskevi Gaki, Elisabete Cruz da Silva, Antoine Combes, Andreas Reisch, Pascal Didier, Andrey Klymchenko

► **To cite this version:**

Deep Sekhar Biswas, Paraskevi Gaki, Elisabete Cruz da Silva, Antoine Combes, Andreas Reisch, et al.. Long-range Energy Transfer Between Dye-loaded Nanoparticles: Observation and Amplified Detection of Nucleic Acids. *Advanced Materials*, 2023, 10.1002/adma.202301402 . hal-04100617

**HAL Id: hal-04100617**

**<https://hal.science/hal-04100617v1>**

Submitted on 17 May 2023

**HAL** is a multi-disciplinary open access archive for the deposit and dissemination of scientific research documents, whether they are published or not. The documents may come from teaching and research institutions in France or abroad, or from public or private research centers.

L'archive ouverte pluridisciplinaire **HAL**, est destinée au dépôt et à la diffusion de documents scientifiques de niveau recherche, publiés ou non, émanant des établissements d'enseignement et de recherche français ou étrangers, des laboratoires publics ou privés.

Long-range energy transfer between dye-loaded nanoparticles: observation and amplified detection of nucleic acids

Deep Sekhar Biswas,<sup>1</sup> Paraskevi Gaki,<sup>1</sup> Elisabete Cruz Da Silva,<sup>1</sup> Antoine Combes,<sup>1</sup> Andreas Reisch,<sup>1</sup> Pascal Didier,<sup>1</sup> and Andrey S. Klymchenko<sup>1,\*</sup>

<sup>1</sup> Laboratoire de Bioimagerie et Pathologies, UMR 7021 CNRS, Faculté de Pharmacie, Université de Strasbourg, 67401 Illkirch, France

\*Corresponding author, email: andrey.klymchenko@unistra.fr

## Abstract

Förster resonance energy transfer (FRET) is essential in optical materials for light-harvesting, photovoltaics and biosensing, but its operating range is fundamentally limited by the Förster radius of  $\sim 5$  nm. Here, FRET between fluorescent organic nanoparticles (NPs) is studied for the first time in order to break this limit. The donor and acceptor NPs are built from charged hydrophobic polymers loaded with cationic dyes and bulky hydrophobic counterions. Their surface is functionalized with DNA in order to control surface-to-surface distance. It is found that the FRET efficiency does not follow the canonic Förster law, reaching 0.70 and 0.45 values for NP-NP distance of 15 and 20 nm, respectively. This corresponds to the FRET efficiency decay as power four of the surface-to-surface NP-NP distance. Based on this long-distance FRET, a DNA nanoprobe is developed, where a target DNA fragment, encoding cancer marker survivin, brings together donor and acceptor NPs at  $\sim 15$  nm distance. In this nanoprobe, a single molecular recognition results in unprecedented color switch for  $>5000$  dyes, yielding a simple and fast assay with 18 attomoles limit of detection. Breaking the Förster distance limit for ultrabright NPs opens the route to advanced optical nanomaterials for amplified FRET-based sensing of biomolecules.

**Keywords:** fluorescent nanomaterials; dye-loaded polymeric nanoparticles; long-range Förster resonance energy transfer; nucleic acid detection; signal amplification.

## 1. Introduction

This article has been accepted for publication and undergone full peer review but has not been through the copyediting, typesetting, pagination and proofreading process, which may lead to differences between this version and the [Version of Record](#). Please cite this article as [doi: 10.1002/adma.202301402](https://doi.org/10.1002/adma.202301402).

This article is protected by copyright. All rights reserved.

Electronic energy transfer is a ubiquitous phenomenon in nature involving light-matter interactions. It is a primary step of photosynthesis, a process responsible for life on our planet, converting solar light energy into chemical energy.<sup>[1]</sup> It also plays a central role in synthetic optical nanomaterials with applications ranging from photovoltaics and artificial photosynthesis,<sup>[2]</sup> to chemical and biological sensing.<sup>[3]</sup> These processes are generally described by Förster resonance energy transfer (FRET) formalism, which assumes that the efficiency of energy transfer decays as the power six of the distance. FRET is one of the most popular approaches for development of functional optical materials, in particular fluorescent probes.<sup>[3a, 3c, 4]</sup> In a typical FRET-based probe, molecular recognition changes the donor-acceptor distance, which leads to a two-color response of the probe, suitable for ratiometric detection of the analyte.<sup>[3b, 4]</sup> The key problem of current molecular probes based on FRET is their insufficient sensitivity within the nanomolar range. This is caused by physically limited brightness of molecular emitters, defined as a product of extinction coefficient and quantum yield, typically below  $300,000 \text{ M}^{-1} \text{ cm}^{-1}$ .<sup>[5]</sup> Detection of disease markers, such as proteins and nucleic acids, requires sensitivity at least in the picomolar range, which is largely below the capacity of dye-based FRET sensors. Therefore, current methods of molecular diagnostics rely on enzymatic amplification schemes such as ELISA<sup>[6]</sup> and PCR.<sup>[7]</sup> Emerging amplification approaches include enzymatic<sup>[8]</sup> and enzyme-free<sup>[9]</sup> molecular amplification schemes, as well as nanotechnology-driven signal amplification approaches, involving plasmonic<sup>[10]</sup> and light-harvesting<sup>[11]</sup> nanomaterials.

Fluorescent nanoparticles (NPs) are particularly promising alternative to organic dyes in the design of FRET sensors, because their brightness can be >100-fold higher, leading to greatly improved signal to background ratio and sensitivity.<sup>[12]</sup> The prominent examples of luminescent NPs as FRET partners in sensing and imaging applications include semiconductor quantum dots (QDs),<sup>[3b]</sup> dye-loaded silica NPs,<sup>[13]</sup> conjugated polymer NPs,<sup>[14]</sup> aggregation-induced emission NPs<sup>[15]</sup> and dye-loaded polymeric NPs.<sup>[16]</sup> However, the general problem of fluorescent NPs is their limited FRET efficiency to a single acceptor, because their size is generally larger than the Förster radius. For example, in the case of QDs, multiple acceptors per particle are needed to achieve efficient FRET in biosensors.<sup>[17]</sup> The second problem is that biosensors for detection of biomolecules frequently need to operate at the distances comparable or longer than the Förster radius, which makes FRET-based approach inefficient. Therefore, significant efforts were done to design nanomaterials that can overcome the Förster distance limit. In particular, advanced materials were developed to achieve light confinement on the nanoscale, such as whispering gallery mode microcavities<sup>[18]</sup> zero-mode waveguides,<sup>[19]</sup> hyperbolic metamaterials<sup>[20]</sup> and plasmonic nanopores,<sup>[21]</sup> allowing long-range energy transfer, sometimes reaching 100 nm distances. Alternatively, excitation energy transfer (EET) in conjugated polymers<sup>[14]</sup> and dye-loaded nanoparticles,<sup>[16a]</sup> allows energy migration within the donor particle that reaches the acceptor over much longer distances than the Förster radius. An attractive approach is to explore energy transfer between donor and acceptor NPs. Previous works showed that the use of gold nanoparticles as energy acceptor with a molecular donor dye resulted in the phenomenon of surface energy transfer (SET), which displayed a decay as a power four of distance, allowing

energy transfer well beyond 10 nm.<sup>[22]</sup> Similar long-range energy transfer was reported for quantum dots as the energy donors and gold NPs as the acceptors.<sup>[23]</sup> However, gold NPs are not emissive and thus cannot be used in ratiometric assays. Semiconductor QDs were also exploited as FRET acceptors,<sup>[24]</sup> but their fundamental limitation is associated to their much stronger absorbance at shorter wavelengths, so their FRET systems suffer from strong direct acceptor excitation. To address the problems above, we considered dye-loaded polymeric NPs as both energy donors and acceptors. Our previous works showed that polymer design allowed tuning the size of NPs in the desired range between 10 and 50 nm,<sup>[25]</sup> while the use of dyes with bulky counterions enabled dye encapsulation with minimized aggregation-caused quenching, yielding bright fluorescent NPs.<sup>[26]</sup> These NPs are particularly suitable as FRET donors, because at high dye loading, the encapsulated dyes undergo ultrafast excitation energy transfer (EET), which was evidenced by nearly-zero steady-state anisotropy and fluorescence anisotropy decay on the fs time scale.<sup>[16a]</sup> Ultrafast EET results in highly efficient FRET from thousands of donor dyes to a single acceptor.<sup>[16a]</sup> This phenomenon of giant light harvesting was successfully applied to the development of nanoprobe for amplified detection of nucleic acids.<sup>[11c, 16b]</sup> However, to achieve efficient FRET in these biosensors, the acceptor molecules had to be placed in direct contact with the polymer surface (Figure 1),<sup>[11c, 16b]</sup> which is not possible in many other biosensing schemes. On the other hand, dye-loaded NPs are expected to be efficient energy acceptors, because their large number of dyes generates high molar absorption coefficient, while their much larger size compared to molecular acceptors could generate phenomena similar to SET with gold NPs as acceptors. Moreover, excitation energy migration within acceptor dyes could provide additional boost to the energy transfer, because the acceptor dyes closer to the donor NP could rapidly transfer energy to more distant dyes within the acceptor NP. However, so far, dye-loaded polymeric NPs have not been explored as donor-acceptor pairs. This could open a unique opportunity to generate FRET nanoprobe operating well beyond the Förster radius and featuring high sensitivity to the biomolecular targets.

Here, we designed dye-loaded polymeric NPs as FRET donors and acceptors and studied energy transfer between them using DNA duplexes to control particle-particle distance. We found that the energy transfer between donor and acceptor NPs can reach 0.45 for ~20 nm distance between their surfaces (~50 nm between the particle centers), which is much higher than the Förster radius (~6.35 nm). Analysis of the distance dependence suggested that NP-NP energy transfer efficiency decays with the fourth power of the particle-particle distance. The observed long-distance FRET can be described by a physical model with a single-molecule donor and a sphere with surface located acceptors or gold nanoparticle. However, in contrast to these systems, our donor is >1000 times brighter (than organic dyes as donors) and its acceptor is emissive (in contrast to non-emissive gold NPs), which is crucial for constructing biosensing materials. Finally, we applied our NP-NP energy transfer system for detection of a nucleic acid fragment, encoding a cancer marker. Despite the long distance between NPs in the sandwich DNA complex (~15 nm), we achieved efficient FRET and sub-picomolar sensitivity to the target nucleic acid, using a fast and simple protocol with robust ratiometric detection.

## 2. Results and discussion

Our donor NPs are composed of hydrophobic poly(methyl methacrylate) (PMMA)- or poly(ethyl methacrylate) (PEMA)-based polymer loaded with the rhodamine based dye salt R18/F5-TPB (Figure 1). Previously, we showed that bulky hydrophobic counterion (F5-TPB) enables high loading of cationic dye R18 in the polymer NPs with minimal aggregation-caused quenching and ultrafast excitation energy migration.<sup>[16a, 26b]</sup> The latter favors efficient transfer energy to one acceptor located at the surface (Figure 1).<sup>[11c]</sup> Here, to achieve long-range FRET, we replaced the acceptor dye molecule with a dye-loaded polymeric NP. For this purpose, we designed a derivative of ATTO647, because, according to our previous work, it was an efficient FRET acceptor dye for R18/F5-TPB-loaded NPs, displaying remarkably high photostability.<sup>[11c]</sup> We synthesized a hydrophobic dye ATTO647-C18 and paired it with the bulky counterion F5-TPB to form acceptor NPs (Figure 1). Two types of NP-NP complexes were prepared. First one is a donor-acceptor NP-NP complex by direct contact of oppositely charged particles, which implies zero distance between the NP surfaces. Second, donor and acceptor NPs functionalized with DNA were hybridized to control NP-NP surface-to-surface distances ranging from 6.8 to 20.4 nm (Figure 1).

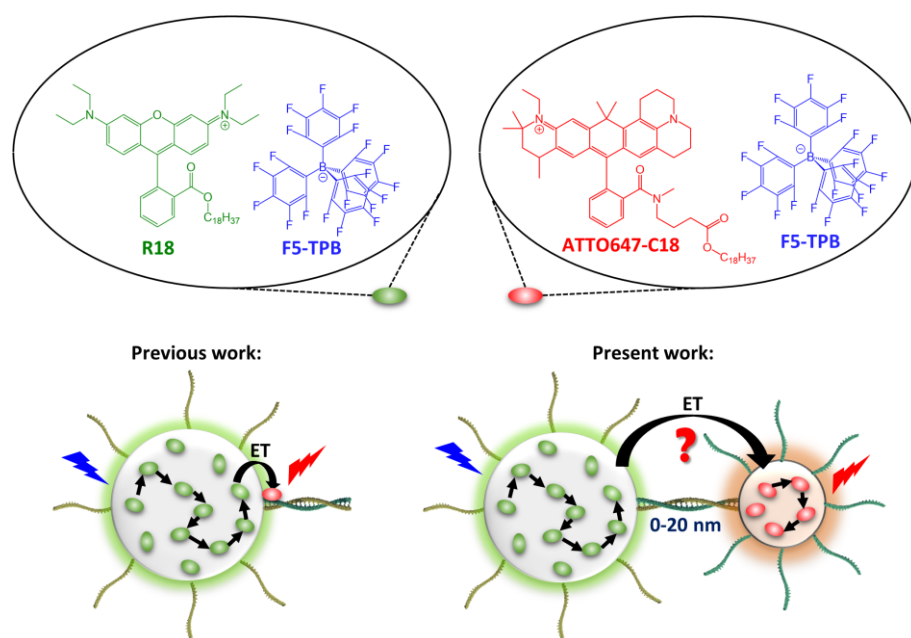


**Figure 1.** Schematic representation of energy transfer (ET) from a dye-loaded nanoparticle to a single acceptor or another dye-loaded nanoparticle. The dye-loaded nanoparticles functionalized with oligonucleotides are schematically presented. Black arrows schematically

show the light-harvesting process toward FRET acceptor. In case of ET between NPs, the distances between NPs were varied from 0 to 20 nm using complementary DNA strands. Chemical structures of the rhodamine derivative R18 with its bulky counterion F5-TPB (in donor NPs) and Atto-647N derivative Atto647-C18 with F5-TPB counterion (in acceptor NPs) are also shown.

In the first approach, the donor NPs were prepared with hydrophobic PMMA-based polymer bearing negatively charged carboxylates (PMMA-MA) and loaded with R18/F5-TPB dye (Figure 2a). The acceptor NPs were prepared from PEMA-based polymer bearing trimethylammonium cationic groups (PEMA-NMe<sub>3</sub>) and loaded with Atto647-C18/F5-TPB (Figure 2a). Donor NPs of two different sizes were prepared by the nanoprecipitation of PMMA-MA polymer with R18/F5-TPB dye (50 wt% loaded with respect to the polymer, i.e. 33 wt% to the total particle mass) in phosphate buffer (PB) at pH 7.4 and in phosphate buffered saline (PBS), which yielded NPs of 68 and 113 nm hydrodynamic diameter, respectively, according to DLS (Table S1). According to TEM, the measured diameters were 40 and 66 nm, respectively (D50%-NP40 and D50%-NP66, respectively, Figure S1, Table S1). The size increase in PBS can be explained by the higher salt concentration in this buffer, which favors formation of larger NPs, in line with our earlier studies.<sup>[25a]</sup> As observed previously, the TEM size, giving the core diameter, was significantly smaller than the hydrodynamic size obtained by DLS.<sup>[16a]</sup> Therefore, here, the TEM data was systematically used for all calculations related to the particle size. The nanoprecipitation of cationic PEMA-NMe<sub>3</sub> in MilliQ water yielded NPs of 14 and 16 nm diameter by TEM for 1 and 30 wt% Atto647-C18/F5-TPB dye loading, respectively (A1%-NP15 and A30%-NP15, respectively, Figure S2, Table S1). The absorption and emission spectra of these two types of acceptor NPs showed minimal variations in the absorption and emission spectra, compared to the Atto647-C18/F5-TPB dye in acetonitrile (Figure S3). Their absorption spectrum overlapped well with the emission spectrum of the donor NPs, which is an important condition for obtaining NP-NP FRET (Figure S3). At both 1 and 30 wt% dye loadings PEMA-NMe<sub>3</sub> NPs displayed relatively high fluorescence quantum yields: 0.40 and 0.21, respectively. Thus, relatively high dye loading can be achieved for Atto647-C18/F5-TPB in the polymeric NPs with minimal aggregation-caused quenching effects, which makes the obtained NPs good candidates as emissive FRET acceptors. To check whether the encapsulated Atto647-C18/F5-TPB dyes undergo EET, we studied their fluorescence anisotropy, which is known to drop due to dye-dye energy hopping.<sup>[26b, 27]</sup> We found that steady-state anisotropy decreased dramatically with the dye loading from  $0.060 \pm 0.001$  at 0.1 wt% loading to  $0.014 \pm 0.004$  and  $0.006 \pm 0.007$  for 1 and 30 wt% loading, respectively, being much smaller than the fundamental anisotropy of Atto647N (0.40).<sup>[28]</sup> Nearly zero fluorescence anisotropy in case of 30 wt% dye loading (the observed value was smaller than the standard error) suggested that the excitation energy redistributed rapidly over the particle, similar to that previously observed for R18/F5-TPB in polymeric NPs.<sup>[16a, 26b]</sup>

Then, to obtain NP-NP donor-acceptor complexes (Figure 2a) the cationic and anionic NPs were mixed together in MilliQ water at 1:2 donor:acceptor ratio and incubated for 1 h at rt before the spectroscopic studies. The fluorescence spectra recorded by exciting the donor NPs (at 530 nm) displayed a strong emission band centered at ~668 nm, corresponding to the acceptor NPs, and only minor contribution of the donor emission (centered at ~585 nm), for both small (40 nm, D50%-NP40) and large (66 nm, D50%-NP66) donor NPs (Figure 2b). The control experiments performed with donor NPs (Control 1: D50%-NP40) excited in the same conditions gave a characteristic single-band donor emission at 580 nm, while the acceptor NPs (Control 2: A30%-NP15) displayed only minor fluorescence due to the direct acceptor excitation at 530 nm (Figure 2b). In the third control experiment, we prepared donor and acceptor NPs using the same PMMA-MA polymer (Figure S4). In this case, both donor and acceptor NPs are negatively charged and, therefore, are not expected to interact. Their mixtures did not show significant acceptor emission (Figure S4), which excluded any contribution of the dye exchange between the donor and acceptor NPs. These observations indicate that, in case of donor and acceptor NPs of opposite charges, the donor-acceptor NP-NP complex was formed, resulting in the efficient FRET between them. To characterize FRET efficiency, we used two approaches. First, the classical approach based on variation of the donor intensity ( $E = 1 - (I/I_0)$ , where  $I$  and  $I_0$  are donor intensities with and without the acceptor). However, in cases when it was difficult to obtain the same concentration of the donor NPs, empirical FRET ratio parameter (so-called proximity ratio) was used, expressed as  $E = I_A/(I_A+I_D)$ , where  $I_A$  and  $I_D$  are peak intensities of the acceptor and donor, respectively, in the fluorescence spectrum.<sup>[29]</sup> The titration of the donor NPs with increased concentration of the acceptor NPs showed that high FRET ratio (>0.97) was achieved already with 1-2 acceptors NPs per donor NP (Figure 2c). The smaller donor NPs (40 nm) showed systematically higher FRET ratio values. According to our previous studies with a single acceptor dye, the smaller size of donor NPs improved FRET efficiency because the propagation length for the donor-donor excitation energy transfer from a randomly excited dye to the particle surface is shorter.<sup>[11c]</sup> Moreover, compared to the previous works, where we used dye molecules as acceptors, for NPs of similar 40-nm size, 23 acceptors at the surface were needed to achieve FRET efficiency ~0.5,<sup>[16b]</sup> while in the most optimized NPs with ~0.5 FRET efficiency to a single acceptor, the particle size was only 16 nm.<sup>[11c]</sup> Here, for ~40 nm donor NPs, we achieved ~0.97 FRET ratio to 1-2 acceptor NP, which is a dramatic improvement in the FRET efficiency.

To understand better the nature of this highly efficient FRET, we studied donor-acceptor NP-NP complex at different loadings of donor (1 and 50 wt%) and acceptor (1 and 30 wt%) dyes. Remarkably, a significant loss in the FRET ratio was observed for NPs with lower donor dye loading (Figure 2d). This effect was observed for different ratios of donor:acceptor NPs (varied concentration of acceptor NPs, Figures 2d and S5). According to our previous fluorescence anisotropy data for the donor NPs<sup>[16a]</sup>, at low dye loading the EET is inefficient, while at high dye loading, ultrafast EET takes place within the encapsulated dyes. Thus, donor-donor EET can explain at least in part the high FRET efficiency. The decrease in the acceptor loading also decreased FRET ratio for both types of donor NPs (Figures 2d and S5),

which indicates that the large number of acceptors in the acceptor NPs is also crucial to achieve a high FRET efficiency.

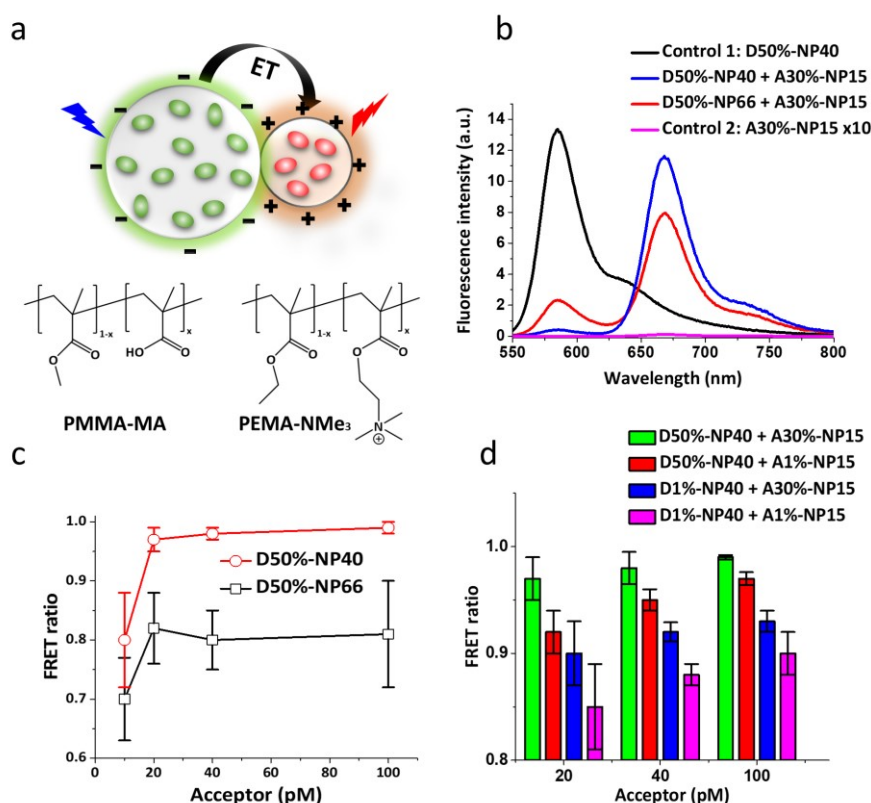


**Figure 2.** FRET between donor and acceptor NPs in direct contact. (a) Schematic representation of anionic and cationic NPs loaded with donor (R18/F5-TPB) and acceptor (Atto647-C18/F5-TPB) dyes respectively, and the chemical formula of the polymers used for the experiment. (b) Steady-state fluorescence spectra of small (40 nm, A50%-NP40) or large (66 nm, D50%-NP66) donor NPs (50 wt% of R18/F5-TPB dye with respect to the polymer) in direct contact with 15 nm acceptor NPs (A30%-NP15, 30 wt% of Atto647-C18/F5-TPB dye with respect to the polymer). For this experiment, the ratio between the donor NP concentration (10 pM) and acceptor NP concentration (20 pM) was 1:2. Controls: 40-nm donor NPs without acceptor NPs (Control 1) and acceptor NPs without donor NPs (Control 2, intensity multiplied 10-fold for visibility), measured at 530 nm (donor) excitation. PBS buffer was systematically used. (c) FRET ratio for the large or small donor NPs (concentration of donor NPs was 10 pM in both cases) measured by varying concentration of the acceptor NPs. (d) FRET ratio of donor (40 nm) and acceptor (15 nm) NPs in direct contact as a function of dye loading (donor NPs: 50 wt% and 1 wt% of R18/F5-TPB dye with respect to the polymer; acceptor NPs: 30 wt% and 1 wt% of Atto647-C18/F5-TPB dye with respect to the polymer). The donor NPs concentration was 10 pM and the acceptor NPs concentrations were 20, 40, 100 pM. All errors are s.d.m. ( $n \geq 3$ ).

Then, to increase the spacing between donor and acceptor NPs, we functionalized them with complementary DNA oligonucleotides (Figure 3a): A20 and T20 oligonucleotides were grafted to donor and acceptor NPs, respectively. Their hybridization is expected to yield a duplex that can ensure surface-to-surface particle spacing of 6.8 nm. The DNA-functionalization is based on our previously developed methodology,<sup>[16b]</sup> which provides high density of grafted DNA and thus proper NP-NP spacing without letting NPs to collapse (Figure 3a). Both donor and acceptor NPs were built from PEMA-AspN3 polymer, allowing preparation of NPs functionalized with azide groups. In case of donor NPs, PEMA-AspN3 polymer and R18/F5-TPB (at 50 wt% loading) were nanoprecipitated in PB at pH 7.4 with 30 mM NaCl, yielding NPs of 64 nm diameter according to DLS and 42 nm according to TEM (Figure 3b,c, Table S1). The increase in the dye loading from 1 to 50 wt% (vs polymer) in these NPs did not produce significant changes in the absorption spectra and they matched well with the excitation spectra (Figure S6). Fluorescence quantum yield decreased with dye loading, but still remained high (0.44) even at 50 wt% vs polymer (Table S2). The average fluorescence lifetime followed the same trend as the QYs with some decrease at 50 wt% loading (Figure S8, Table S2), in line with an earlier work on PMMA-based NPs.<sup>[16a]</sup> Thus, at high loading, the dyes remain highly emissive with spectroscopic properties close to the molecular form. For 50 wt% dye loading with respect to the polymer, 42-nm particle is expected to contain 5600 dyes per particle, making it highly fluorescent. Moreover, at this high dye loading, PEMA-AspN3 NPs exhibited nearly zero fluorescence anisotropy suggesting ultrafast EET within the encapsulated dyes, important for efficient FRET to a single acceptor.<sup>[11c]</sup> The acceptor NPs were prepared from PEMA-AspN3 with Atto647-C18/F5-TPB dye (30 wt% dye loading) by nanoprecipitation in PB at pH 7.4 without additional salt. This condition yielded smaller acceptor NPs: 26 nm diameter according to TEM (Figure 3b,c, Table S1), which corresponds to ~800 acceptor dyes per NP. Their QY remained good (0.19), similar to that observed before the cationic PEMA-based NPs. Both donor and acceptor PEMA-AspN3 NPs were sufficiently photostable, as continuous irradiation under standard excitation power density of the fluorometer resulted in rather small changes in the emission intensity over 30 min (Figure S8).

The obtained donor (D50%-NP40) and acceptor (A30%-NP25) NPs bearing azide groups at the surface were then coupled with corresponding DNA oligonucleotides bearing reactive DBCO group: A20-DBCO and T20-DBCO, respectively. Mixing A20-functionalized donor NPs with T20-functionalized acceptor NPs is expected to yield the DNA duplex, where the surfaces of NPs are separated by a distance of ~6.8 nm, close to the Förster radius for the couple of parent dyes rhodamine B and Atto647N (6.35 nm<sup>[30]</sup>). The mixtures of donor and acceptor NPs with varied concentrations of the acceptor NPs were incubated to achieve hybridization of their complementary DNA strands and the FRET spectra were recorded. Already at a 1:1 ratio of the donor NPs to the acceptor NPs, we observed a nearly complete loss of the donor emission together with appearance of the acceptor emission corresponding to a FRET efficiency of 0.97 (Figure 3d,e). Further increase in the acceptor concentration provided only a minor increase in the FRET efficiency, which reached 0.99. In contrast, a control experiment, where both donor and acceptor NPs were functionalized with A20

oligonucleotide, gave almost negligible FRET signal (Figure 3f). The latter suggests that the contribution of non-specific interactions within A20-functionalized NPs, exchange of encapsulated dyes and direct excitation of the acceptor can be excluded, so that the observed efficient FRET originates from specific hybridization of donor A20-NPs and acceptor T20-NPs. One should note that here we observed comparable FRET efficiency to that for the direct contact between NPs (see above). Given that the distance between surfaces of the donor and acceptor NPs is close to the Förster radius for the Rhodamine-Atto647 pair (6.35 nm), the observed FRET efficiency close to 100% is clearly much higher than the efficiency predicted by the Förster model for a single donor-single acceptor pair. The donor-acceptor NP complexes were also visualized by fluorescence microscopy (Figure S9). The control donor NPs showed mainly emission at the donor channel, while in the presence of acceptor NPs, the donor channel intensity dropped, and the acceptor emission became dominant. As a result, in the merged images, the color of NPs switched from green to red, which confirmed formation of FRET complexes of NPs. Presence of more intense spots in these images may indicate presence of larger aggregates of donor and acceptor NPs.

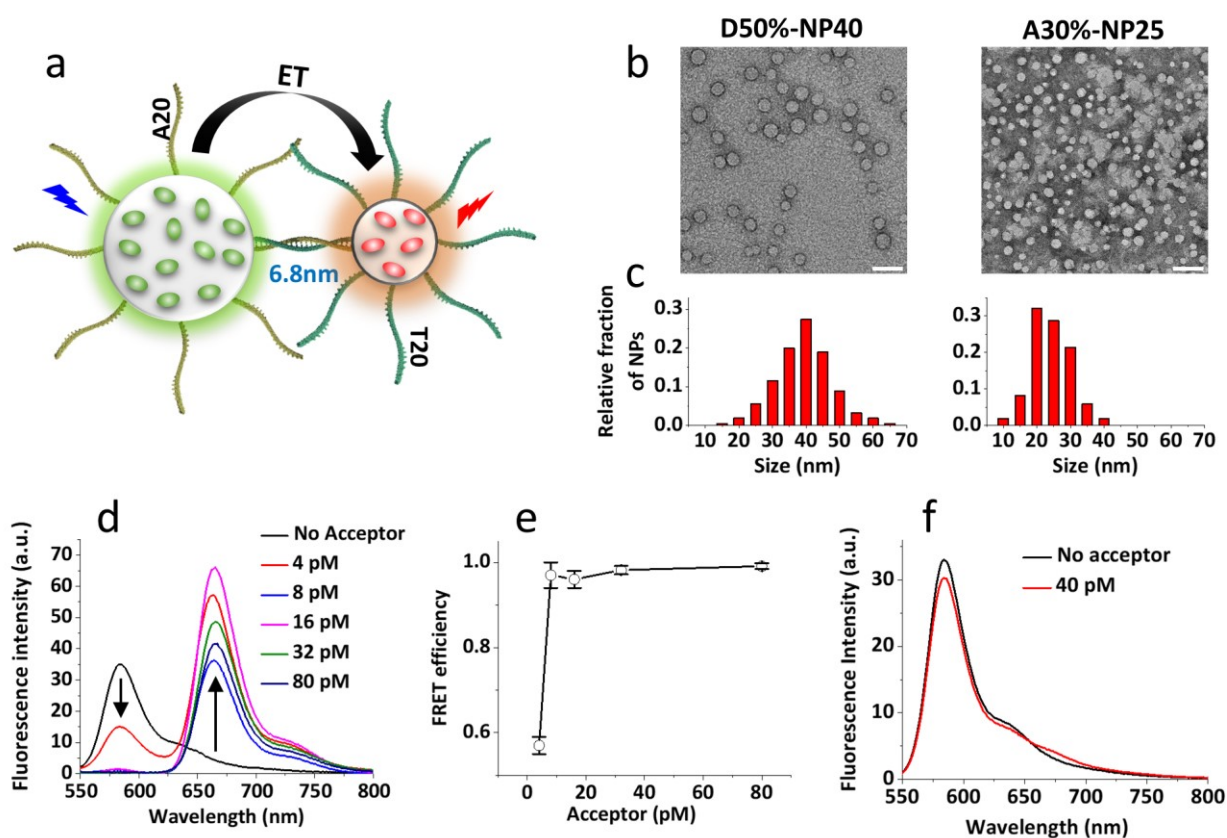


**Figure 3.** FRET between donor and acceptor NPs at distance of 20 base pairs (6.8 nm). (a) Schematic representation of A20 and T20 DNA-modified NPs loaded with donor (R18/F5-TPB) and acceptor (Atto647-C18/F5-TPB) dyes, respectively. (b) TEM images of individual NPs (containing 50 wt% of R18/F5-TPB dye with respect to the polymer for donor NPs and 30 wt% of Atto647-C18/F5-TPB dye with respect to the polymer for acceptor NPs) before their modification with DNA. The donor NPs were prepared in phosphate buffer with 30 mM

NaCl (pH 7.4) and the acceptor NPs were prepared in phosphate buffer (pH 7.4) without NaCl. ~200 NPs were analyzed per condition. Scale bars: 100 nm. (c) size distributions of the donor and acceptor NPs. (d) Steady-state fluorescence spectra of A20-modified donor NPs (40 nm) with varied concentration of T20-modified acceptor NPs (25 nm). (e) FRET efficiencies for donor NPs (40 nm) with varied concentration of the acceptor NPs (25 nm). The donor NPs concentration was 8 pM. All errors are s.d.m. ( $n \geq 3$ ). (f) Control experiment for non-interacting NPs: fluorescence spectra of A20-modified donor NPs (40 nm) with 40 nM A20-modified acceptor NPs (25 nm). The donor NPs concentration was 8 pM. HEPES (Mis-B) buffer was systematically used. Excitation wavelength was 530 nm.

In the view of this unexpectedly high FRET efficiency, we next tuned the surface-to-surface distance between NPs using other hybridization schemes. To increase the distance nearly twice (to 14.9 nm), we used a sandwich hybridization scheme, where 23 nt oligonucleotide on the donor NP and 21 nt oligonucleotide on the acceptor NP were hybridized through a linking sequence of 45 nt complementary to these two oligonucleotides (44 bp length for the two duplexes, Figure 4a). Then, we also designed a pair of complementary sequences of 60 nt, which is expected to further increase the NP-NP surface-to-surface distance, corresponding to the duplex length of 20.4 nm. We incubated the donor and acceptor NPs and then measured the FRET spectra and corresponding FRET efficiency. For both NP-NP distances studied, the increase in the concentration of the acceptor NPs resulted in rapid increase in the FRET efficiency, which reached relatively stable values starting from concentrations corresponding to 1:2 ratio of the donor NPs to acceptor NPs (Figures 4b and S10). When all NP-NP distances were compared for the 1:2 ratio, the FRET efficiency was similarly high for 0 and 6.8 nm (0.96-0.97) and then decreased for longer NP-NP distances, reaching values of 0.70 and 0.45 at 14.9 and 20.4 nm, respectively. We also studied time-resolved emission decays of the donor NPs in the 1:2 donor-acceptor complexes at different NP-NP distances and obtained very similar values of FRET efficiency as those in the steady-state measurements (Figure 4c and S11, S12).

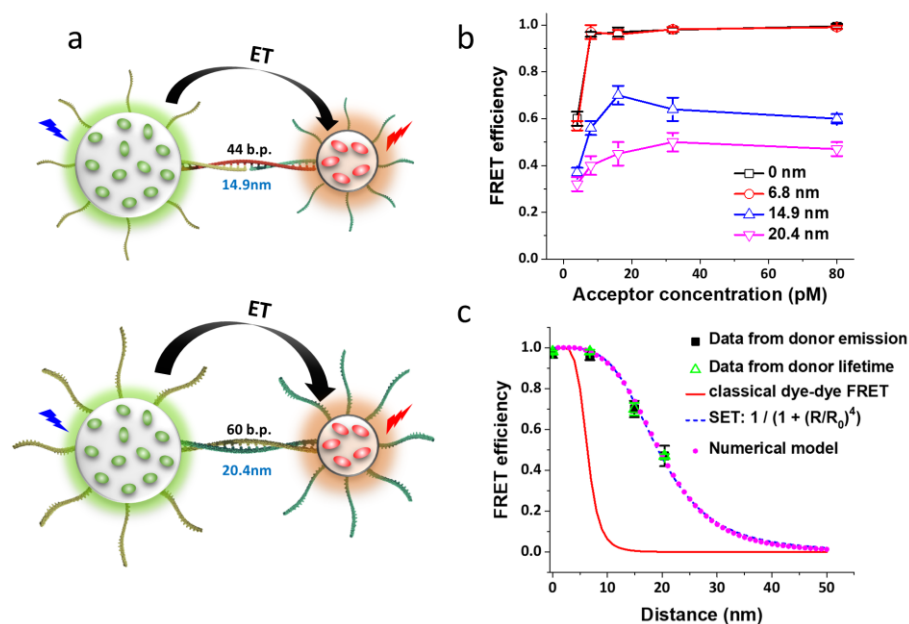


**Figure 4.** FRET between donor and acceptor NPs at different distances. (a) Schematic representation of DNA-modified NPs loaded with donor (R18/F5-TPB) and acceptor (Atto647-C18/F5-TPB) dyes. The distance between donor and acceptor NPs were controlled by the length of DNA duplexes. (b) FRET efficiencies between DNA-modified NPs (containing 50 wt% of R18/F5-TPB dye with respect to the polymer for the 40 nm donor NPs and 30 wt% of Atto647-C18/F5-TPB dye for the 25 nm acceptor NPs) at different distances (20, 44 and 60 b.p. corresponding to 6.8, 14.9 and 20.4 nm). The case of direct NP-NP contact (0 nm) is also shown. The donor NP concentration was 8 pM. HEPES (Mis-B) buffer was systematically used. All errors are s.d.m. ( $n \geq 3$ ). (c) FRET efficiencies between these NPs measured using both steady-state (black squares) and time-resolved (green triangles) spectroscopy as a function of their surface-to-surface distance. The magenta points correspond to the FRET efficiencies calculated using the numerical model described in the Materials and Methods section. The blue curve corresponds to the analytical models developed previously for lipidic systems.<sup>[31]</sup> All errors are s.d.m. ( $n \geq 3$ ).

These high values of FRET efficiencies between NPs are clearly above the values expected from the Förster theory for classical single donor-single acceptor pair. Indeed, assuming that FRET takes place from surface to surface of NPs, FRET efficiency for 6.8 nm spacing would be  $< 0.5$  according to the Förster law (for the Förster radius of 6.35 nm), whereas in our case, it is  $\sim 0.97$ . Moreover, for 14.9 and 20.4 nm distance, the Förster theory predicts nearly zero FRET efficiency, while we observe values of 0.70 and 0.45, respectively. In addition, if we calculate the distance between the centers of NPs, the NP distances would be 26.0, 40.6, 48.7 and 54.2 nm, which would lead to nearly zero FRET efficiency for all our NP-NP couples, including that with the direct contact without DNA. As a consequence, the decrease in the transfer efficiency in case of NP-NP FRET does not follow a power of six law, as it would be

the case for single donor-single acceptor pair (Figure 4c). This deviation from the standard Förster model has already been observed for FRET between a dye and gold NPs, where the energy transfer efficiencies decrease with distance to the fourth power.<sup>[22]</sup> Remarkably, the distance dependence in our system also scales with the fourth power of the distance (Figure 4c), although the materials used here are completely different from those in the previous report. To account for the energy transfer between a single donor and a single acceptor, Förster formalism uses the point-dipole approximation. However, when the acceptors are homogeneously distributed over a surface, one has to integrate the FRET rate between each donor-acceptor pairs over 2 dimensions giving rise to a power four dependence with respect to the distance, as previously demonstrated.<sup>[32]</sup> In particular, the fourth power distance dependence was described with an analytical model proposed earlier to account for the energy transfer between donors and acceptors embedded in lipid bilayers.<sup>[31]</sup> A numerical model based on this approach was adapted to our system. In our approach, the FRET efficiency was calculated as a function of the distance between a single donor and a half-sphere with homogeneously distributed acceptors at the surface (Figure S13). In this case, the donor can transfer its excitation energy to each individual acceptor with a rate given by the Förster theory ( $k_{\text{FRET}} \propto r^{-6}$ , Figure S13). The steady-state fluorescence intensities of the donor and acceptors are determined by solving a set of coupled differential equations (see Materials and Methods). We found that the increase in the number of acceptors per surface of 20 nm half-sphere increased the deviation from the Förster law towards longer distances (Figure S14). However, to match the experimental observations the number of acceptors homogeneously distributed over the surface of the half-sphere must be  $\sim 10,000$  (Figure 4c and S13), far above the real number of acceptor dyes loaded within our acceptor NPs. Indeed, the 26-nm acceptor NP encapsulates  $\sim 800$  dyes (i.e. only  $\sim 400$  dyes in a half-sphere) and they are distributed all over the volume of the particle, so that the effective number of acceptors at its surface is even lower. Thus, even though some previous reports and the numerical model could match the current experimental observations, our NP-NP FRET system presents unprecedented features. First, the donor is not a point emitter, but a nanoparticle containing thousands of dyes within a radius far beyond the Förster distance. Second, our acceptor NP requires much less dyes than the theoretical prediction and they can be distributed all over the particle volume. This unique behavior could be explained by ultrafast excitation energy transfer within both donor and acceptor NPs. Indeed, our previous works showed that due to ultrafast EET within the encapsulated dyes,<sup>[16a]</sup> the excitation energy propagates within the donor NPs beyond the Förster radius and ensures efficient FRET from hundreds encapsulated dyes to a single acceptor attached to the NP surface.<sup>[11c]</sup> Therefore, the donor NP can be considered as a single emitter that can transfer energy from the NP surface (Figure 1). On the other hand, in the acceptor NP, the dyes located closer to the surface are coupled by fast EET with the all-other encapsulated dyes, as evidenced by the anisotropy data (see above). Therefore, after initial transfer to the NPs surface, the excitation energy can rapidly redistribute over other parts of NPs (Figure 1), which should boost the performance of the acceptor NPs. Thus, the numerical model with multiple acceptors combined with the ultrafast EET within both donor and acceptor NPs could explain why in our system the energy transfer

is essentially surface-to-surface processes characterized by high efficiency at long NP-NP distances, which, to the best of our knowledge, has not been reported yet for particle-particle FRET.

The observed phenomenon of long-distance NP-NP FRET is of outmost importance for biosensing applications. Here, based on it, we developed an assay for nucleic acid sensing. We took our DNA sandwich system, where the energy transfer between NPs is induced in the presence of the 45 nt linking oligonucleotide (Figure 4a). The latter is our “target” oligonucleotide, which corresponds to a fragment of mRNA of survivin, a key anti-apoptotic protein overexpressed in cancer cells, serving as important cancer biomarker.<sup>[33]</sup> In this assay, the mixture of the donor and acceptor NPs without the target oligonucleotide is not expected to undergo FRET, while the presence of the target should induce formation of the donor-acceptor pair (with 14.9 nm spacing) that undergoes FRET (Figure 5a). However, using Atto647-C18 as acceptor led to a small contribution of the direct excitation of the acceptor present in excess, so that even without target DNA, some background signal from the acceptor emission was observed (Figure S15). Therefore, we changed the acceptor to Cy5-based dye DiD with bulky counterion F5-TPB, which was shown to exhibit efficient encapsulation and bright emission inside polymeric NPs.<sup>[34]</sup> The acceptor NPs were formulated exactly as for the Atto647-C18 NPs, with 30 wt% dye loading (vs polymer), yielding NPs of 17 nm size by TEM (Figure S16, Table S1), which were further functionalized with corresponding oligonucleotides. In this case, at the donor-acceptor NP-NP ratio 1:2, no signs of the acceptor emission were observed (Figure 5b), which implies negligible direct excitation of acceptor and minimal non-specific interaction between the donor and acceptor DNA-functionalized NPs. The addition of increasing concentrations of the target DNA led to a gradual increase in the relative intensity of the acceptor emission centered at ~670 nm. Thus, as expected, the target DNA triggers the formation of donor-acceptor NP-NP pair and turns on the acceptor emission. The FRET ratio showed gradual growth with increase in the target DNA concentration in total RNA extract from cells (Figure 5c), which suggests that this approach allows detection of specific oligonucleotides. Estimation of a limit of detection (LOD), based on three standard deviations without the target, gave a value of 0.36 pM. Considering that the detection volume was 50  $\mu$ L, the LOD expressed in absolute amount of the oligonucleotide was 18 attomol. The obtained LOD values are significantly lower compared to those we previously observed for our FRET system with a single dye acceptor (1-5 pM).<sup>[11c, 35]</sup> Moreover, in this case, the detection process is much faster: 1h instead of 6h incubation.

Multiple reasons can explain the much better performance of the present FRET system. First, this is a turn-on system where the target induces the appearance of FRET signal, in contrast to that in the previous DNA strand-displacement assays, which are based on the loss of FRET.<sup>[11c, 16b]</sup> Second, all capture nucleic acids attached to the surface of NPs are complementary to the target, whereas in the previous assays the capture oligonucleotides corresponded to a small fraction mixed with the excess of non-coding (A20) oligonucleotides.<sup>[11c, 16b]</sup> This implies much higher effective concentration of the capture

DNA and, therefore, faster kinetics of hybridization (i.e. less incubation time) for the new assay. It is clear that this NP-NP FRET detection assay can be further optimized for improving its sensitivity and it can be further applied for specific biomedical applications, which will be a subject of our future studies. Here, we provide the first proof-of-concept of exploiting long-range energy transfer between NPs for the biomolecular sensing. It is important to stress that in this case the single molecular recognition event (i.e. hybridization of the target sequence) induces formation of a donor-acceptor NP-NP pair that switches the emission of >5000 dyes inside donor particle to the emission of the acceptor particle with comparable intensity (Figure 5), owing to efficient energy transfer over 15-nm surface-to-surface distance. Previous reports of efficient energy transfer from a large ensembles of emitters to a single acceptor, for instance using dye-loaded polymeric NPs<sup>[11c, 16a]</sup> and upconversion NPs,<sup>[36]</sup> were limited to short distances with acceptors placed directly on the particle surface. To the best of our knowledge, this is the first report showing that one molecular recognition event can trigger efficient energy transfer from so large dye ensemble to an acceptor beyond Forster distance, which enables unrepresented signal amplification in the fluorescence sensing.

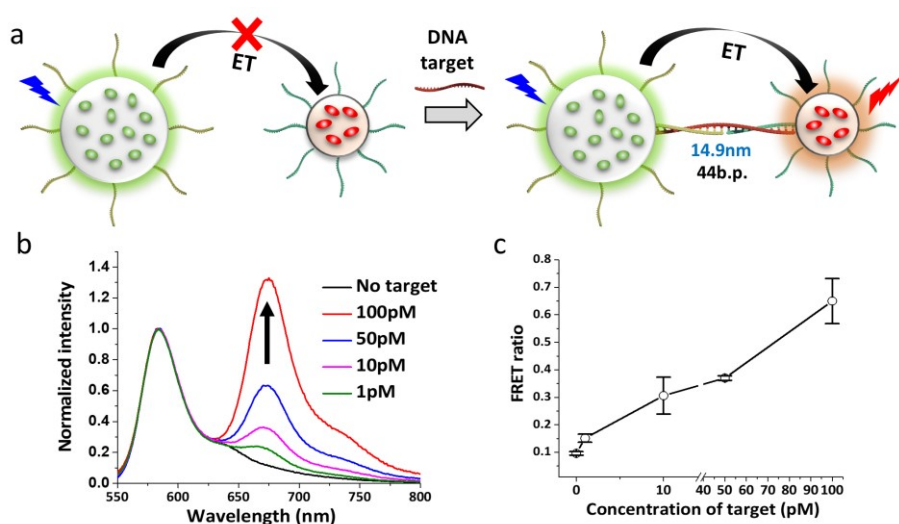


**Figure 5.** Response of the NP-NP FRET assay to the nucleic acid target. (a) Schematic representation of DNA-modified NPs loaded with donor (50 wt% of R18/F5-TPB) and acceptor (30 wt% of DiD/F5-TPB) dyes at surface-to-surface distance of 14.9 nm. The target DNA is represented in red color. Normalized steady-state fluorescence spectra (b) and corresponding FRET ratios (c) for the donor (8 pM) and acceptor (16 pM) NPs with varied concentration of the nucleic acid target. HEPES (Mis-B) buffer containing total RNA extract from cells (0.01 g/L) was used. All errors are s.d.m. ( $n \geq 3$ ).

### 3. Conclusions

Excitation energy transfer is essential in the development of optical materials for light-harvesting, photovoltaic and biosensing applications. In particular, long-range energy transfer in nanomaterials is a route to biosensors with high brightness and sensitivity to the target, important for molecular diagnostics applications. The present work is the first study of energy transfer between two fluorescent organic nanoparticles, which demonstrates that the excitation energy can propagate far beyond the Förster radius. We designed polymeric NPs loaded with donor or acceptor dyes and studied energy transfer between them at different distances controlled by DNA duplexes. We found that the FRET efficiency does not follow the canonic Förster law as a power six of distance, reaching 0.70 and 0.45 for 15 and 20 nm surface-to-surface distances between NPs. FRET efficiency in our NP-NP systems decays as a power four of the distance, which was previously reported for a single dye emitter as the donor and a gold NP as the acceptor.<sup>[22]</sup> Based on the previous works on the lipid bilayers,<sup>[31]</sup> we developed a numerical model for FRET from a single dye emitter to a half-sphere with surface-located acceptors. However, it suggested that the power four distance dependence can be only achieved when the number of acceptors on the surface of NPs is much higher than we actually use in our acceptor NPs (10,000 dyes vs 400 actually used for a half-sphere). Thus, our NP-NP FRET system presents a number of unprecedented features. First, its donor contains >5000 dyes and, thus, it is much brighter than a single dye emitter, owing to strong light-harvesting capacity of this dye ensemble and high fluorescence quantum yield. Second, its acceptor is an emissive nanoparticle (unlike gold NP) and it requires much less dyes distributed all over NP, unlike the numerical model above. These unique features can be explained by ultrafast excitation energy migration (EET) within dyes in both donor and acceptor NPs, which ensures that the energy transfer between NPs takes place from the surface of the donor NP to the surface of the acceptor NP. Indeed, EET brings the excitation energy to the surface of the donor NP and then, after energy transfer to the surface of the acceptor NP, the EET can further spread it to the acceptor dyes all over the particle. On the other hand, in comparison to existing advanced materials that allow light confinement at the nanoscale,<sup>[18-21]</sup> our long-distance FRET nanomaterials feature simplicity and flexibility. Indeed, our system is essentially based on functionalized donor and acceptor polymeric NPs and their FRET response can be measured both in solution and on surfaces using a variety of fluorescence techniques.

As a proof-of-concept, we applied this NP-NP FRET system for the detection of a DNA fragment encoding cancer marker survivin. The donor and acceptor NPs were functionalized with sequences complementary to the two parts of this fragment, so that they could get together in a sandwich-like complex at a distance of ~15 nm. We found that the DNA-functionalized donor and acceptor NPs did not interact by themselves, whereas presence of the 45 nt DNA target triggered a ratiometric response, observed as an increase in the FRET signal vs the donor signal. Titration experiments with the DNA target revealed a limit of detection of 0.36 pM, which corresponded to 18 attomoles in the absolute amount. In comparison to the previous FRET probes based on these NPs as donors and single dye

acceptors,<sup>[11c]</sup> much higher sensitivity was achieved for significantly shorter incubation times. Owing to the high FRET efficiency beyond the Förster radius in this NP-NP system, a single molecular recognition of the target leads to response of >5000 dyes with color switch from donor to acceptor emission. This is an outstanding amplification that has not been achieved for any kind of optical biosensing material to date. Moreover, the color switching will enable robust ratiometric detection of the target using relatively simple detection setups, including portable fluorometers and plate readers. On the other hand, the remaining challenges of this long-distance FRET system, based exclusively on organic NPs, are potential aggregation of NPs, their photostability and multiplexing capabilities. Finally, given such long energy transfer distances, our NP-NP FRET system could be adapted to other detection schemes including those using antibodies. This work is currently in progress and will be reported in due course.

## 4. Materials and Methods

### 4.1. Materials

PMMA-MA (1.6% methacrylic acid,  $M_n$  15,000;  $M_w$  34,000), acetonitrile (anhydrous, spectroscopic grade, 99.8%), rhodamine B octadecyl ester perchlorate (>98.0%), potassium tetrakis(pentafluorophenyl)borate, HEPES sodium salt, potassium chloride (KCl), magnesium chloride ( $MgCl_2$ ), potassium carbonate and octadecyl iodide were purchased from Sigma-Aldrich. 1,1'-dioctadecyl-3,3,3',3'-tetramethylindodicarbocyanine perchlorate (DiD) and LabTek chambers (Borosilicate cover glass, eight wells) were purchased from ThermoFisher Scientific and Atto647N carboxylic acid were purchased from ATTO-TEC. Sodium phosphate dibasic dihydrate (>99.0%) and sodium phosphate monobasic (>99.0%), both were purchased from Sigma-Aldrich and used to prepare 20 mM phosphate buffers at pH 7.4 and pH 9.2. Dulbecco's phosphate buffered saline were purchased from Dominique Dutscher. Amicon Centrifugal filters (0.5mL, 100kD) were purchased from Sigma-Aldrich. For saline buffer, sodium chloride ( $\geq 99\%$ , Sigma Aldrich) 30 mM was added to 20 mM phosphate buffer and pH was adjusted to pH 7.4 with sodium hydroxide 1M solution. Milli-Q water (Millipore) was used in all the experiments. Protein LoBind Eppendorfs were purchased from Eppendorf.

### 4.2. Nucleic acids sequences

Lyophilized single strand DNA sequences were purchased from Biomers GmbH, dissolved in Milli-Q water, aliquoted and stored at -20 °C for further experiments. The oligonucleotide sequences used in this study are shown below.

DNA:

A20-DBCO, 5'-AAA AAA AAA AAA AAA AAA AA - (DBCO)-3'.

T20-DBCO, 5'-TTT TTT TTT TTT TTT TTT TT-(DBCO)-3'.

T20-Biotin, 5'-TTT TTT TTT TTT TTT TTT TT-(Biotin)-3'

Sur1-DBCO, 5'-(DBCO)-ACT CAT GGG GTC GTC ATC TGG CT -3'.

Sur2-DBCO, 5'-CCC AGC CTT CCA GCT CCT TGA - (DBCO)-3'.

Sur-target, 5'-TTC AAG GAG CTG GAA GGC TGG GAG CCA GAT GAC GAC CCC ATG AGA-3'

60nt1-DBCO, 5'-CAC TGA TGC TAT ACG GCT GAT GAC TAT CGA ATT CGG TAG TAG GCG AGC TCC TTC ATA GGC- (DBCO)-3'.

60nt2-DBCO, 5' GCC TAT GAA GGA GCT CGC CTA CTA CCG AAT TCG ATA GTC ATC AGC CGT ATA GCA TCA GTG - (DBCO)-3'.

### 4.3. Synthesis

Rhodamine B octadecyl ester tetrakis(pentafluorophenyl)borate (R18/F5-TPB) was synthesized by ion exchange and purified by column chromatography as explained earlier.<sup>[26b]</sup> Synthesis of DiD/F5-TPB was also performed using ion exchange and purification by column chromatography as described previously.<sup>[34]</sup> Synthesis of PEMA-AspN3 was performed using peptide coupling method as described previously.<sup>[11c]</sup> Synthesis of PMMA-NMe<sub>3</sub> 1% was described previously.<sup>[37]</sup>

#### 4.3.1. Synthesis of octadecyl A647N (Atto647-C18)

Atto647N carboxylic acid (2 mg, 2.7  $\mu\text{mol}$ ) was dissolved in dry dimethylformamide (DMF) then octadecyl iodide (10 mg, 27  $\mu\text{mol}$ ) and potassium carbonate (5 mg, 37  $\mu\text{mol}$ ) were added to it. The reaction mixture was heated at 60 °C overnight in the dark. Then, it was cooled and concentrated under reduced pressure to remove DMF and re-dissolved in dichloromethane (DCM) then washed thoroughly with brine. Then the DCM part was concentrated under reduced pressure and then purified with preparatory thin layer chromatography and dried over argon atmosphere. Final yield was 87% (2.13 mg). HRMS (ESI),  $m/z$ :  $[M]^+$  calculated for  $\text{C}_{60}\text{H}_{88}\text{N}_3\text{O}_3^+$ , 898.6821; found, 898.6828.

#### 4.3.2. Synthesis of Atto647-C18/F5-TPB

Atto647N-C18 (2mg 2.3  $\mu\text{mol}$ ) was mixed with potassium tetrakis(pentafluorophenyl)borate (5 mg, 7  $\mu\text{mol}$ ) in dichloromethane and acetonitrile (1:1) mixture. Then it was cooled and concentrated under reduced pressure to remove DMF and re-dissolved in dichloromethane (DCM) then washed thoroughly with brine. Then the DCM part was purified with column chromatography and the dried over argon atmosphere. Final yield was 80% (2.97 mg). HRMS (ESI),  $m/z$ :  $[M]^+$  calculated for  $\text{C}_{60}\text{H}_{88}\text{N}_3\text{O}_3^+$ , 898.6821; found, 898.6830.

#### 4.3.3. Synthesis of fluorescent NPs

The NPs were prepared by nanoprecipitation method describe previously.<sup>[25b, 26b]</sup> For preparation of PMMA-MA NPs (anionic NPs), the stock solutions of PMMA-MA in acetonitrile (2 mg/mL) were prepared containing different amount of R18/F5-TPB (1 and 50 wt% relative to the polymer weight; i.e. 50 wt% corresponds to 1:2 dye to polymer ratio). Then, 50  $\mu$ L of these stock solutions were diluted quickly using micropipette to 500  $\mu$ L of 20 mM phosphate buffer (PB) at pH 7.4, r.t under vigorous shaking (Thermomixer in 1,150 rpm). Next, these NP suspensions were again quickly diluted to 1 mL with the same PB (20 mM, pH 7.4) at r.t. For the larger-sized NPs, Dulbecco's Phosphate Buffered Saline (PBS) was used only at the first dilution step. For the smaller-sized NPs, phosphate buffer at pH 9.2 was used only at the first dilution step.

For the preparation of cationic NPs, different amounts of Atto647-C18/F5-TPB in acetonitrile (1 and 30 wt% relative to the polymer weight) were added to the polymer (PEMA-NMe<sub>3</sub> 1%) solution (2 mg/mL) in acetonitrile. Then, 50  $\mu$ L of these stock solutions were diluted quickly using micropipette to 500  $\mu$ L of Milli-Q water, r.t under vigorous shaking (Thermomixer in 1,150 rpm). Next, these NP suspensions were again quickly diluted to 1 mL with the same Milli-Q water at r.t.

PEMA-AspN<sub>3</sub> NPs were obtained by nanoprecipitation with 20 mM PB at pH 7.4 with 30 mM of NaCl: 50  $\mu$ L of the polymer solution in acetonitrile (2 mg/mL with a required wt% of R18/F5-TPB relative to the polymer i.e. from 0.1, 1, 5 and 50 wt% for R18/F5-TPB and 30 wt% of Atto647-C18/F5-TPB or DiD/F5-TPB) were then added quickly using a micropipette to 450  $\mu$ L of PB (with 30mM NaCl for R18/F5-TPB NPs and without NaCl for Atto647-C18/F5-TPB or DiD/F5-TPB NPs) under shaking with Thermomixer (1,150 rpm). Next, these NP suspensions were again quickly diluted to 1 mL with the same phosphate buffer respectively, at r.t. Then, the residues of acetonitrile were evaporated under reduced pressure.

#### 4.3.4. Synthesis of DNA-modified NPs

Aliquots of A20-DBCO, T20-DBCO, Sur1-DBCO, Sur2-DBCO, 60nt1-DBCO and 60nt2-DBCO (20  $\mu$ M) were added to 100  $\mu$ L of corresponding nanoparticles. Then, they were mixed carefully, microcentrifuged and kept overnight (18 h) at 40 °C in incubator chamber without shaking protected from light. After the mixtures were cooled down to r.t. Then, these reaction mixtures were purified by centrifugation using centrifuge filters (Amicon, 0.5 mL, 100 kDa) on 1000 rcf at 20 °C for 5 min. The procedure of centrifugation was repeated 4 times to remove the non-reacted oligonucleotides. The obtained nanoprobe in a volume of 0.5 mL were kept in the dark at 4 °C.

#### 4.4. Characterization of NPs

The hydrodynamic diameters of the NPs were measured using dynamic light scattering (DLS) on a Zetasizer Nano ZSP (Malvern Instruments). The mean values were obtained from three sets of results based on volume distribution analysis.

Transmission electron microscopy (TEM) was performed to further characterize the NPs. Carbon-coated copper-rhodium electron microscopy grids with a 300 mesh (Euromedex, France) were surface treated with a glow discharge in amylamine atmosphere (0.5 mbar, 4 – 5 mA, 30 s) in an Elmo glow discharge system (Cordouan Technologies, France). Then, 5  $\mu\text{L}$  of the solution of NPs at 0.04 g/L were deposited on the grids and left for 5 min. The grids were then treated for 1 min with a 2% uranyl acetate solution for staining. After that, the experiments were performed on a Philips CM120 transmission electron microscope equipped with a LaB6 filament and operating at 100 kV. Images were analyzed using Fiji software.

Absorption spectra were recorded on a Cary 5000 scan UV-vis spectrophotometer (Varian); and emission spectra and fluorescence anisotropy were recorded on a FS5 spectrofluorometer (Edinburg Instruments) equipped with thermostated compartment. The fluorescence spectra the NPs were recorded at the excitation wavelength of 530 nm (for R18/F5-TPB NPs) and 620 nm (DiD/F5-TPB and Atto647-C18/F5-TPB NPs). The QYs of the NPs were measured using rhodamine 101 (QY=1.00)<sup>[38]</sup> (for R18/F5-TPB NPs) and DiD in methanol as a reference (QY=0.33) (for DiD/F5-TPB and Atto647-C18/F5-TPB NPs).<sup>[39]</sup>

For photostability experiments, 50  $\mu\text{L}$  of the donor or acceptor NPs (50 pM concentration of NPs) were placed in 3 $\times$ 3 mm black quartz cuvette and kept under continuous light illumination 530 or 640 nm, respectively, with power density 0.2 mW/cm<sup>2</sup>. Their fluorescence was measured at 580 or 660 nm, respectively.

#### 4.5. Estimation of the concentration of DNA-modified NPs

We calculated the volume of the NPs using the diameter measured by TEM. Then, we estimated how many dye molecules are there per nanoparticle. By the loading of the dye into the NPs (30 wt% or 50 wt%), we estimated the number of moles of the dye present in the unit volume of a particle. These values are multiplied with Avogadro's number to estimate the number of dye molecules per particle (Table S1). Then, based on the absorption spectrum of NPs and known molar extinction coefficient of dyes (125,000 M<sup>-1</sup> cm<sup>-1</sup> for R18, 150,000 M<sup>-1</sup> cm<sup>-1</sup> for Atto647-C18, and 250,000 M<sup>-1</sup> cm<sup>-1</sup> for DiD), we estimated the concentration of NPs in solution as

$$\frac{\text{absorbance}}{\text{number of dyes per NPs} \times \text{extinction coefficient}}$$

This concentration of NPs was used for all the particle-particle FRET experiments.

#### 4.6. Particle-particle complexes for FRET studies

For direct contact FRET experiment, the aliquots of Atto647-C18/F5-TPB PMMA-NMe<sub>3</sub> (A1%-NP15 or A30%-NP15) NPs at indicated concentration were added to R18/F5-TPB

PMMA-MA (D1%-NP40, D50%-NP40 or D50%-NP66) NPs (10 pM) in PBS to the final volume of 50  $\mu$ L in LoBind Eppendorfs. Then the mixture was kept for 1h in the Thermomixer (300 rpm) protected from light at r.t. Finally, steady state spectra were recorded after diluting the mixtures to 500  $\mu$ L.

For FRET between DNA-modified NPs, the aliquots of Atto647-C18/F5-TPB PEMA-AspN<sub>3</sub> (A30%-NP25-N3) NPs, bearing T20 DNA or 60nt2 DNA, at indicated concentration were added to R18/F5-TPB PEMA-AspN<sub>3</sub> (D50%-NP40-N3) NPs (8 pM), bearing, respectively, A20 DNA or 60nt1 DNA, in HEPES (Mis-B, see below) buffer to the final volume of 50  $\mu$ L in LoBind Eppendorfs. Then, the mixture was kept for 65 min at 50 °C protected from light. After the mixtures were cooled down to r.t. Finally, steady state spectra were recorded after diluting the mixtures to 500  $\mu$ L. Mis-B buffer contained 12 mM of HEPES buffer along with 120 mM of KCl and 0.4 mM of MgCl<sub>2</sub> at pH 7.4.

For FRET between DNA-modified NPs (with 44 b.p.), the aliquots of Atto647-C18/F5-TPB PEMA-AspN<sub>3</sub> (A30%-NP25-N3) NPs, bearing Sur2 DNA, were added to R18/F5-TPB PEMA-AspN<sub>3</sub> (D50%-NP40-N3) NPs (8 pM), bearing Sur1 DNA, and 500 pM of 45 nt (target) DNA sequence (Sur-target) in HEPES (Mis-B) buffer to the final volume of 50  $\mu$ L in LoBind Eppendorfs. Then, the mixture was kept for 65 min at 50 °C protected from light. After the mixtures were cooled down to r.t. Finally, steady state spectra were recorded after diluting the mixtures to 500  $\mu$ L.

#### 4.7. Estimation of limit of detection (LOD)

For LOD calculation, 8 pM of donor NPs D50%-NP40-N3, bearing Sur1 DNA were mixed with 16 pM of acceptor NPs A30%-NP17-N3 (prepared with DiD/F5-TPB dye), bearing Sur2 DNA, in 50  $\mu$ L of HEPES (Mis-B) buffer containing 0.01 g/L RNA extract (HeLa) in LoBind Eppendorfs. After different concentrations of 45 nt DNA target (Sur-target) were added to the mixture. Then, the mixture was kept for 1h at 50 °C protected from light. After the mixtures were cooled down to r.t. Then, the steady state spectra were recorded after diluting these mixtures to 100  $\mu$ L, using a micro-cuvette. These experiments were performed thrice to construct the calibration curve (Figure 5). The intermediate dilution of nucleic acid target was done in Milli-Q water containing 0.01mg/mL Tween 80. RNA extraction from HeLa cells was performed as previously described.

#### 4.8. Fluorescence lifetime measurements

Time-resolved fluorescence measurements were performed using time-correlated single-photon counting (TCSPC) technique. Excitation pulses at 532 nm were generated by a supercontinuum laser (NKT Photonics SuperK Extreme) with 10 MHz repetition rate. The fluorescence decays were collected at 585 nm, using a polarizer set at magic angle and a 16 mm band-pass monochromator (Jobin Yvon). The single-photon events were detected with a micro-channel plate photomultiplier R3809U Hamamatsu, coupled to a pulse pre-amplifier

HFAC (Becker-Hickl GmbH) and recorded on a time-correlated single photon counting board SPC-130 (Becker-Hickl GmbH). The instrumental response function (IRF) recorded with a polished aluminum reflector showed a full-width at half-maximum of 70 ps for 532 nm excitation.

Time-resolved exponential decays were fitted by using the global fit procedure of Igor Pro (Wavemetrics). The fitting function was a sum of exponential decays (up to 4 components) convolved with a normalized Gaussian curve of standard deviation  $\sigma$  standing for the temporal IRF and a Heavy side function. All emission decays were fitted using a weighting that corresponds to the standard deviation of the photon number squared root.

#### 4.9. Calculation of FRET Efficiency and FRET ratio

FRET efficiencies were calculated using the following equation

$$E = 1 - \frac{I_{D-A}}{I_D} = 1 - \frac{\tau_{D-A}}{\tau_D}$$

Where E is FRET efficiency,  $I_{D-A}$  is fluorescence intensity donor in presence of acceptor and  $I_D$  is fluorescence intensity donor without acceptor;  $\tau_{D-A}$  is average lifetime of donor in presence of acceptor and  $\tau_D$  is average lifetime of donor without acceptor.

FRET ratio was calculated using the following equation

$$FRET\ ratio = \frac{A}{D + A}$$

Where A is the fluorescence intensity of acceptor and D is the fluorescence intensity of donor of same NPs.

#### 4.10. Distance dependent FRET efficiency data fitting

Distance dependent FRET efficiency data were fitted by using the Igor Pro (Wavemetrics). For FRET efficiencies (E) between single donor and single acceptor system the classical FRET formula was used:

$$E = \frac{1}{1 - \left(\frac{r}{R}\right)^6}$$

where r is the distance between donor and acceptor chromophores and R is the characteristic distance (the Förster distance or Förster radius) with a 50% transfer efficiency.<sup>[40]</sup>

To account for our experimental observations, a numerical simulation was used to calculate the FRET efficiencies as a function of the distance between a single donor and the surface of a sphere where the acceptors are homogeneously distributed on its surface. In this case, the

donor can transfer its excitation energy to each individual acceptor at a rate given by the Förster theory ( $k_{\text{FRET}} \propto r^{-6}$ ). The steady state intensities of the donor and acceptor NP were determined by the solving the following set of differential equations:

$$\left\{ \begin{array}{l} \frac{dD_0}{dt} = -k_{exc} \cdot e^{-\left(\frac{t-t_0}{\sigma}\right)^2} D_0 + \frac{D_1}{\tau_D} \\ \frac{dD_1}{dt} = k_{exc} \cdot e^{-\left(\frac{t-t_0}{\sigma}\right)^2} D_0 - \frac{D_1}{\tau_D} - n_1 k_1 A_1 - \dots - n_n k_n A_n \\ \frac{dA_1}{dt} = k_1 A_1 - \frac{A_1}{\tau_A} \\ \vdots \\ \frac{dA_n}{dt} = k_n A_n - \frac{A_n}{\tau_A} \end{array} \right.$$

Where  $k_{exc}$  is the excitation rate of the donor dye, in this model we used a 10 ps pulsed gaussian excitation ( $e^{-\left(\frac{t-t_0}{\sigma}\right)^2}$ ).  $\tau_D$  and  $\tau_A$  are the fluorescence lifetimes of the donor (4 ns) and acceptor (2,4 ns) respectively.  $D_0$  and  $D_1$  are the ground and first excited state of donor,  $A_n$  stands for the first excited state of acceptors. The energy transfer rates are calculated using the following equation:

$$k_n = \frac{1}{\tau_D} \left( \frac{R_0}{d_n} \right)^6$$

Where  $R_0$  is the Förster radius (6.35 nm),  $\tau_D$  the fluorescence lifetimes of the donor (4 ns) and  $d_n$  the distance between the donor and the  $n^{\text{th}}$  localized on the surface of the acceptor NP. The distances were calculated by using a spherical reference frame.  $n_n$  corresponds to the number of acceptor dyes localized at the distance equal to  $d_n$  (i.e. considering the surface density of acceptor dyes).

The FRET efficiency for a given configuration was calculated using the ratio of the total intensity emitted by the acceptors and the total intensity emitted by the acceptors plus the donor:

$$E = \frac{k_r^A (\sum_n \int A_n(t) dt)}{k_r^A (\sum_n \int A_n(t) dt) + k_r^D \int D_1(t) dt}$$

The radiative rates have been estimated from the fluorescence lifetimes of the dyes and their quantum yield. In the simulation, we considered up to 10 distances and the number of acceptors dyes was changed to account for the experimental FRET values (Figure 4c).

For surface energy transfer efficiencies, the following formula was used:

$$E_S = \frac{1}{1 - \left(\frac{d}{D}\right)^4}$$

where  $d$  is the distance between donor and acceptor and  $D$  is the distance at which SET efficiency decreases to 50% (i.e., equal probability of energy transfer and spontaneous emission).<sup>[22]</sup>

#### 4.11. Single-particle measurements

For single particle FRET measurements, the LabTek chambers were incubated with 1M KOH solution followed by extensive washing with Milli-Q water. Then, 100  $\mu$ L of 0.5 mg/mL BSA-biotin solution in autoclaved Milli-Q water were added in each chamber of the LabTek. After 20 min of incubation the chamber was washed 3 times with PBS and then was incubated with 100  $\mu$ L of 0.5mg/mL neutravidin solution in PBS for 15 min. Following that, the chamber was cleaned thoroughly with PBS, and then, it was incubated with 200  $\mu$ L of 1  $\mu$ M solution of T20-biotin in PBS for 20 min and subsequently washed with PBS. After that, 100  $\mu$ L of the D-A20-NP40/A-T20-NP25 complexes were added and incubated for 45 min followed by cleaning with PBS and finally the surface of each chamber was fully covered by PBS.

Single-particle measurements were performed in the epi-fluorescence mode using Nikon Ti-E inverted microscope with a 60x objective (Apo TIRF, oil, NA 1.49, Nikon). The excitation was provided by light emitting diodes (SpectraX, Lumencor) at 550 nm for R18/F5-TPB and 640 nm for Atto647-C18/F5-TPB. To have multi-channel image detection, corresponding to R18/F5-TPB and Atto647-C18/F5-TPB signals, different filters were used (600 $\pm$ 50nm for R18/F5-TPB and 705 $\pm$ 72nm for Atto647-C18/F5-TPB). Single-particle analysis was performed using the Fiji software.

#### Acknowledgements

This work was supported by Agence nationale de la recherche (ANR) grant ANR-19-CE09-0006, the European Research Council ERC Consolidator Grant BrightSens 648525 and ERC Proof of Concept Grant AmpliFISH 899928. We thank Tanushree Gupta for advices with nanoparticles preparation and Corinne Crucifix from the FRISBI platform for her help with the electron microscopy.

#### Conflicts of interests

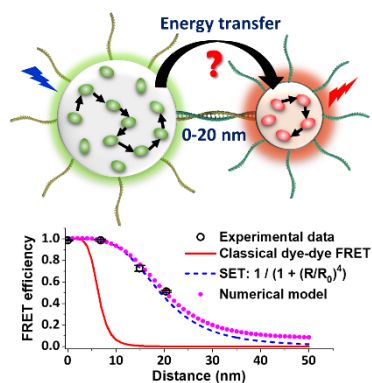
ASK and AR deposited a patent protecting this technology and they are co-founders of BrightSens Diagnostics SAS.

## 5. References

- [1] T. Mirkovic, E. E. Ostroumov, J. M. Anna, R. van Grondelle, Govindjee, G. D. Scholes, *Chemical Reviews* **2017**, *117*, 249.
- [2] G. J. Hedley, A. Ruseckas, I. D. W. Samuel, *Chemical Reviews* **2017**, *117*, 796.
- [3] a) W. R. Algar, N. Hildebrandt, S. S. Vogel, I. L. Medintz, *Nat. Methods* **2019**, *16*, 815; b) N. Hildebrandt, C. M. Spillmann, W. R. Algar, T. Pons, M. H. Stewart, E. Oh, K. Susumu, S. A. Diaz, J. B. Delehanty, I. L. Medintz, *Chem. Rev.* **2017**, *117*, 536; c) K. E. Sapsford, L. Berti, I. L. Medintz, *Angew. Chem. Int. Ed.* **2006**, *45*, 4562.
- [4] L. Yuan, W. Y. Lin, K. B. Zheng, S. S. Zhu, *Accounts of Chemical Research* **2013**, *46*, 1462.
- [5] J. B. Grimm, L. D. Lavis, *Nature Methods* **2022**, *19*, 149.
- [6] R. M. Lequin, *Clinical Chemistry* **2005**, *51*, 2415.
- [7] a) B. Kaltenboeck, C. Wang, *Adv Clin Chem* **2005**, *40*, 219; b) R. Higuchi, C. Fockler, G. Dollinger, R. Watson, *Biotechnology (N Y)* **1993**, *11*, 1026.
- [8] a) M. M. Ali, F. Li, Z. Zhang, K. Zhang, D.-K. Kang, J. A. Ankrum, X. C. Le, W. Zhao, *Chemical Society Reviews* **2014**, *43*, 3324; b) R. Deng, K. Zhang, J. Li, *Accounts of Chemical Research* **2017**, *50*, 1059; c) J. S. Gootenberg, O. O. Abudayyeh, M. J. Kellner, J. Joung, J. J. Collins, F. Zhang, *Science* **2018**, *360*, 439.
- [9] a) R. M. Dirks, N. A. Pierce, *Proceedings of the National Academy of Sciences* **2004**, *101*, 15275; b) F. C. Simmel, B. Yurke, H. R. Singh, *Chemical Reviews* **2019**, *119*, 6326.
- [10] a) A. Puchkova, C. Vietz, E. Pibiri, B. Wünsch, M. Sanz Paz, G. P. Acuna, P. Tinnefeld, *Nano Letters* **2015**, *15*, 8354; b) S. E. Ochmann, C. Vietz, K. Trofymchuk, G. P. Acuna, B. Lalkens, P. Tinnefeld, *Analytical Chemistry* **2017**, *89*, 13000; c) J. Luan, A. Seth, R. Gupta, Z. Wang, P. Rathi, S. Cao, H. Gholami Derami, R. Tang, B. Xu, S. Achilefu, J. J. Morrissey, S. Singamaneni, *Nature Biomedical Engineering* **2020**, *4*, 518.
- [11] a) Y. Jiang, J. McNeill, *Chemical Reviews* **2017**, *117*, 838; b) W. Wu, G. C. Bazan, B. Liu, *Chem* **2017**, *2*, 760; c) N. Melnychuk, S. Egloff, A. Runser, A. Reisch, A. S. Klymchenko, *Angewandte Chemie-International Edition* **2020**, *59*, 6811.
- [12] a) O. S. Wolfbeis, *Chem. Soc. Rev.* **2015**, *44*, 4743; b) P. D. Howes, R. Chandrawati, M. M. Stevens, *Science* **2014**, *346*, 1247390; c) A. Reisch, A. S. Klymchenko, *Small* **2016**, *12*, 1968; d) H. Q. Peng, L. Y. Niu, Y. Z. Chen, L. Z. Wu, C. H. Tung, Q. Z. Yang, *Chemical Reviews* **2015**, *115*, 7502.
- [13] D. Genovese, E. Rampazzo, S. Bonacchi, M. Montalti, N. Zaccheroni, L. Prodi, *Nanoscale* **2014**, *6*, 3022.
- [14] a) Y. Jiang, J. McNeill, *Chem. Rev.* **2017**, *117*, 838; b) W. B. Wu, G. C. Bazan, B. Liu, *Chem* **2017**, *2*, 760.
- [15] X. H. Wang, N. Song, W. Hou, C. Y. Wang, Y. Wang, J. Tang, Y. W. Yang, *Advanced Materials* **2019**, *31*.
- [16] a) K. Trofymchuk, A. Reisch, P. Didier, F. Frasc, P. Gilliot, Y. Mely, A. S. Klymchenko, *Nat. Photonics* **2017**, *11*, 657; b) N. Melnychuk, A. S. Klymchenko, *J. Am. Chem. Soc.* **2018**, *140*, 10856.
- [17] a) I. L. Medintz, A. R. Clapp, H. Mattoussi, E. R. Goldman, B. Fisher, J. M. Mauro, *Nat. Mater.* **2003**, *2*, 630; b) A. R. Clapp, I. L. Medintz, J. M. Mauro, B. R. Fisher, M. G. Bawendi, H. Mattoussi, *Journal of the American Chemical Society* **2004**, *126*, 301.
- [18] S. Jana, X. Xu, A. Klymchenko, A. Reisch, T. Pons, *ACS Nano* **2021**, *15*, 1445.

- [19] a) M. Baibakov, S. Patra, J.-B. Claude, A. Moreau, J. Lumeau, J. Wenger, *ACS Nano* **2019**, *13*, 8469; b) M. Baibakov, S. Patra, J.-B. Claude, J. Wenger, *ACS Omega* **2020**, *5*, 6947.
- [20] W. D. Newman, C. L. Cortes, A. Afshar, K. Cadien, A. Meldrum, R. Fedosejevs, Z. Jacob, *Science Advances* **2018**, *4*, eaar5278.
- [21] a) X. Zambrana-Puyalto, N. Maccaferri, P. Ponzellini, G. Giovannini, F. De Angelis, D. Garoli, *Nanoscale Advances* **2019**, *1*, 2454; b) X. Zambrana-Puyalto, P. Ponzellini, N. Maccaferri, D. Garoli, *Physical Review Applied* **2020**, *14*, 054065.
- [22] C. S. Yun, A. Javier, T. Jennings, M. Fisher, S. Hira, S. Peterson, B. Hopkins, N. O. Reich, G. F. Strouse, *Journal of the American Chemical Society* **2005**, *127*, 3115.
- [23] a) T. Pons, I. L. Medintz, K. E. Sapsford, S. Higashiya, A. F. Grimes, D. S. English, H. Mattoussi, *Nano Letters* **2007**, *7*, 3157; b) A. Samanta, Y. Zhou, S. Zou, H. Yan, Y. Liu, *Nano Letters* **2014**, *14*, 5052.
- [24] a) K. F. Chou, A. M. Dennis, *Sensors (Basel)* **2015**, *15*, 13288; b) M. Chern, R. Toufanian, A. M. Dennis, *Analyst* **2020**, *145*, 5754.
- [25] a) A. Reisch, D. Heimbürger, P. Ernst, A. Runser, P. Didier, D. Dujardin, A. S. Klymchenko, *Advanced Functional Materials* **2018**, *28*; b) A. Reisch, A. Runser, Y. Arntz, Y. Mely, A. S. Klymchenko, *ACS Nano* **2015**, *9*, 5104.
- [26] a) B. Andreiuk, A. Reisch, E. Bernhardt, A. S. Klymchenko, *Chem.-Asian J.* **2019**, *14*, 836; b) A. Reisch, P. Didier, L. Richert, S. Oncul, Y. Arntz, Y. Mely, A. S. Klymchenko, *Nature Communications* **2014**, *5*, 4089.
- [27] R. Camacho, D. Täuber, I. G. Scheblykin, *Advanced Materials* **2019**, *31*, 1805671.
- [28] S. Sharma, K. Chakraborty, B. K. Müller, N. Astola, Y. C. Tang, D. C. Lamb, M. Hayer-Hartl, F. U. Hartl, *Cell* **2008**, *133*, 142.
- [29] a) S. Preus, L. M. Wilhelmsson, *ChemBioChem* **2012**, *13*, 1990; b) R. Bouchaala, L. Mercier, B. Andreiuk, Y. Mély, T. Vandamme, N. Anton, J. G. Goetz, A. S. Klymchenko, *J Control Release* **2016**, *236*, 57.
- [30] <https://www.fpbases.org/fret/>, accessed: 2023.
- [31] a) P. K. Wolber, B. S. Hudson, *Biophysical Journal* **1979**, *28*, 197; b) T. G. Dewey, G. G. Hammes, *Biophysical Journal* **1980**, *32*, 1023.
- [32] a) P. Bastiaens, A. de Beus, M. Lacker, P. Somerharju, M. Vauhkonen, J. Eisinger, *Biophysical Journal* **1990**, *58*, 665; b) H. Kuhn, *The Journal of Chemical Physics* **1970**, *53*, 101; c) H. Kuhn, D. Möbius, *Angewandte Chemie International Edition in English* **1971**, *10*, 620.
- [33] R. A. Olie, A. P. Simões-Wüst, B. Baumann, S. H. Leech, D. Fabbro, R. A. Stahel, U. Zangemeister-Wittke, *Cancer Res* **2000**, *60*, 2805.
- [34] B. Andreiuk, A. Reisch, M. Lindecker, G. Follain, N. Peyrieras, J. G. Goetz, A. S. Klymchenko, *Small* **2017**, *13*, 1701582.
- [35] S. Egloff, N. Melnychuk, A. Reisch, S. Martin, A. S. Klymchenko, *Biosens Bioelectron* **2021**, *179*, 113084.
- [36] J. Zhou, C. Li, D. Li, X. Liu, Z. Mu, W. Gao, J. Qiu, R. Deng, *Nature Communications* **2020**, *11*, 4297.
- [37] A. Combes, K.-N. Tang, A. S. Klymchenko, A. Reisch, *Journal of Colloid and Interface Science* **2022**, *607*, 1786.
- [38] W.-J. Li, X.-Q. Wang, D.-Y. Zhang, Y.-X. Hu, W.-T. Xu, L. Xu, W. Wang, H.-B. Yang, *Angewandte Chemie International Edition* **2021**, *60*, 18761.
- [39] I. Texier, M. Goutayer, A. Da Silva, L. Guyon, N. Djaker, V. Josserand, E. Neumann, J. Bibette, F. Vinet, *J Biomed Opt* **2009**, *14*, 054005.
- [40] A. K. Wozniak, G. F. Schröder, H. Grubmüller, C. A. Seidel, F. Oesterhelt, *Proc Natl Acad Sci U S A* **2008**, *105*, 18337.

## TOC graphic



**Breaking FRET limit:** operating range of FRET is fundamentally limited by the Förster radius of  $\sim 5$  nm. The study on dye-loaded fluorescent polymeric nanoparticles connected by DNA duplexes of different lengths reveals efficient energy transfer far beyond the Förster radius, following power-four distance dependence. This phenomenon is applied for amplified detection of a target nucleic acid with attomole sensitivity.